

Cellular inhibition of Chk2 kinase and potentiation of camptothecins and radiation by the novel Chk2 inhibitor PV1019

Andrew G. Jobson, George T. Lountos, Philip L. Lorenzi, Jenny Llamas, John Connelly, David Cerna, Joseph E. Tropea, Akikazu Onda, Gabriele Zoppoli, Sudhir Kondapaka, Guangtao Zhang, Natasha J. Caplen, John H. Cardellina II, Stephen S. Yoo, Anne Monks, Christopher Self, David S. Waugh, Robert H. Shoemaker and Yves Pommier

Laboratory of Molecular Pharmacology, Center for Cancer Research, National Cancer Institute, NIH, Bethesda MD 20892-4255, USA (AGJ, PLL, JL, AO, GZ and YP). Macromolecular Crystallography Laboratory, National Cancer Institute, NIH, Frederick MD 21702-1201, USA (GTL, JET and DSW). Laboratory of Functional Genomics, SAIC-Frederick, NCI-Fredrick, Frederick MD 21702, USA (JC and AM). Screening Technologies Branch, Developmental Therapeutics Program, Division of Cancer Treatment and Diagnosis, National Cancer Institute, NIH, Frederick MD 21702-1201, USA (SK, JHC and RHS). Provid Pharmaceuticals, North Brunswick, NJ 08902 (GZ and CS). Molecular Radiation Therapeutics Branch, SAIC-Frederick, NCI-Fredrick, Frederick MD 21702, USA (DC). Molecular Radiation Therapeutics Branch, Radiation Research Program (RRP), Division of Cancer Treatment and Diagnosis (DCTD), National Cancer Institute, NIH, Rockville, MD 20892-7440, USA (SSY). Gene Silencing Section, Genetics Branch, Center for Cancer Research, National Cancer Institute, NIH, Bethesda, MD, 20892-4260, USA (NJC).

Running Title: Inhibition of Chk2 kinase by PV1019

Corresponding author:

Yves Pommier, M.D, Ph.D.

Chief, Laboratory of Molecular Pharmacology

Center for Cancer Research

National Cancer Institute

NIH, Bethesda, MD 20892-4255

Tel: 301-496-5944

Fax: 301-402-0752

Email: pommier@nih.gov Web: <http://discover.nci.nih.gov/pommier/pommier.htm>

Text pages: 27

Tables: 1

Figures: 6

Abstract words: 200

Introduction words: 743

Discussion words: 1079

References: 40

Recommended section: Cellular and molecular

Standard abbreviations: ATM: ataxia telangiectasia mutated; CPT: camptothecin; IR: ionizing radiations; Top1: topoisomerase I; TPT: topotecan.

Abstract

Chk2 is a checkpoint kinase involved in the ATM pathway, which is activated by genomic instability and DNA damage, leading to either cell death (apoptosis) or cell cycle arrest. Chk2 provides an unexplored therapeutic target against cancer cells. We recently reported NSC 109555 as a novel chemotype Chk2 inhibitor. We have now synthesized a derivative of NSC 109555, PV1019 (NSC 744039), which is a selective sub-micromolar inhibitor of Chk2 *in vitro*. The co-crystal structure of PV1019 bound in the ATP binding pocket of Chk2 confirmed enzymatic/biochemical observations that PV1019 acts as a competitive inhibitor of Chk2 with respect to ATP. PV1019 was found to inhibit Chk2 in cells. It inhibits Chk2 autophosphorylation (which represents the cellular kinase activation of Chk2), Cdc25C phosphorylation, and HDMX degradation in response to DNA damage. PV1019 also protects normal mouse thymocytes against IR-induced apoptosis, and it shows synergistic antiproliferative activity with topotecan, camptothecin, and radiation in human tumor cell lines. We also show that PV1019 as well as Chk2 siRNA can exert antiproliferative activity themselves in the cancer cells with high Chk2 expression in the NCI60 screen. These data indicate that PV1019 is a potent and selective inhibitor of Chk2 with chemotherapeutic and radiosensitization potential.

Introduction

Chk2 kinase is pivotal in mediating the DNA damage signal following genotoxic stress, leading to either DNA repair or apoptosis, depending on the severity of the damage and the genetic background of the cells. In addition, it has been proposed that Chk2 functions as a barrier to tumorigenesis by maintaining genomic stability as the DNA-damage response is activated early in cancer lesions, and this DNA damage induction is thought to prevent or delay genetic instability and tumorigenesis (Bartkova et al., 2005; Gorgoulis et al., 2005). Following DNA damage, Chk2 is primarily activated by ATM and DNA-PK via phosphorylation of Thr68 on Chk2 (Ahn et al., 2000), which in turn causes homodimerization and subsequent trans-activating autophosphorylations of Thr383 and Thr387 (Ahn and Prives, 2002) and cis-phosphorylation of Ser516 (Wu and Chen, 2003). Following activation, Chk2 phosphorylates a number of downstream substrates involved in various cellular processes, including cell cycle arrest, apoptosis, DNA repair and mitosis. For a comprehensive overview of these interactions see (Pommier et al., 2005; Pommier et al., 2006) and <http://discover.nci.nih.gov/mim>.

There are a number of studies suggesting therapeutic value of Chk2 inhibitors [for review see (Pommier et al., 2005; Antoni et al., 2007)]. The primary rationale for targeting Chk2 in cancer therapy would be combination with genotoxic agents. Antisense inhibition of Chk2 increased apoptosis in p53-defective HEK293 cells (Yu et al., 2001). Down regulation of Chk2 augmented the effect of paclitaxel in MCF7 cells (Chabaliere-Taste et al., 2008). Chk2 inhibition also enhanced the level of mitotic catastrophe when used in

combination with either doxorubicin (Castedo et al., 2004) or cisplatin (Vakifahmetoglu et al., 2008). In addition, Chk2 siRNA down regulation or a dominant negative form of Chk2 (Chk2-DN) prevented the release of the anti-apoptotic factor survivin from the mitochondria, thus augmenting ionizing radiation (IR)- or doxorubicin-induced apoptosis (Ghosh et al., 2006). Furthermore, doxycycline-induced expression of Chk2-DN potentiated the cytotoxic effect of doxorubicin in HCT116 xenografts in mice. In addition to augmenting the effect of cytotoxic drugs, Chk2 inhibitors may elicit radio/chemoprotection of normal tissue via abrogation of p53-dependent apoptosis (Pommier et al., 2005; Antoni et al., 2007). In support of this, Chk2-null mice are viable, but show increased survival when exposed to ionizing radiation (Hirao et al., 2000; Takai et al., 2002). That effect has also been demonstrated using Chk2 inhibitors in either mouse thymocytes (Carlessi et al., 2007) or isolated CD4⁺ and CD8⁺ human lymphocytes (Arienti et al., 2005).

An additional rationale for the therapeutic development of Chk2 inhibitors is because of increased levels of activated Chk2 in some human tumor cells. It is plausible that cells where Chk2 is constitutively activated have adapted and become addicted to Chk2 in order to survive. In that situation, inhibition of Chk2 may cause cell death. Activated Chk2 has also been found important in viral replication. Specifically, down regulation of Chk2 by short hairpin RNA in cells infected with hepatitis C led to abrogation of viral replication (Ariumi et al., 2008). Furthermore, the ATM-mediated DNA damage response pathway has been implicated in HIV viral replication (Lau et al., 2005). Small molecule inhibition of ATM caused a decrease in HIV viral replication, again suggesting a role for

the ATM-Chk2 pathway in viral replication and a benefit for anti-viral therapy with a Chk2 inhibitor.

Only a few selective Chk2 inhibitors have been reported: NSC 109555 (Jobson et al., 2007), 2-arylbenzimidazole (Arienti et al., 2005), VRX0466617 (Carlessi et al., 2007) and a series of isothiazole carboxamides (Larson et al., 2007); and none are known to be under clinical development. However, many more dual Chk1/Chk2 inhibitors are known—debromohymenialdisine (DBH) (Curman et al., 2001), DBH analogue (Sharma and Tepe, 2004), XL-844 (Matthews et al., 2007), AZD7762 (Zabludoff et al., 2008), and PF-473336 (Ashwell et al., 2008), with the final three compounds currently undergoing early clinical evaluation. Of these three compounds, AZD7762 is approximately equipotent against Chk1 and Chk2, whereas PF-477736 and XL-844 are more selective against Chk1 than Chk2 (Lapenna and Giordano, 2009). The occurrence of dual Chk1/Chk2 inhibitors is not unexpected given that Chk1 and Chk2 are part of the CAMK kinase family in the kinome (Manning et al., 2002). Recent insights into co-crystal structures of Chk2 inhibitors bound in the ATP binding pocket of Chk2 will enable improved, selective drug design.

Here we present both *in vitro* and cellular data showing selective inhibition of Chk2 in biochemical and cellular assays, and potentiation of cytotoxic agents and radiation by a novel Chk2 inhibitor PV1019.

Methods

Expression and purification of recombinant proteins

The expression and purification of recombinant Chk2 and Cdc25C has been described in detail elsewhere (Yu et al., 2002; Jobson et al., 2007). Recombinant Chk1 was purchased from Upstate (Charlottesville, VA). Histone H1, from calf thymus, was purchased from Roche (Indianapolis, IN).

Protein kinase assays

In vitro protein kinase assays were performed as previously described with minor modifications (Jobson et al., 2007). Drugs were dissolved in DMSO, in which case the final DMSO concentration in assays was 1% and the controls were performed under comparable conditions. Chk2 protein kinase activity, measured as ^{32}P incorporation into Chk2, GST-Cdc25C or histone H1, was determined using a PhosphorImager (Molecular Dynamics, Sunnyvale, CA). Densitometry was performed using ImageQuant (GE Healthcare Piscataway, NJ). For competitive inhibition studies Chk2 was incubated with GST-Cdc25C for 10 minutes at 30°C. The ratio of 'cold' ATP and ^{32}P -labeled γ -ATP was kept constant while the concentration was altered, 100, 50, 40 and 25 μM . This set of reactions was repeated in the presence of 0.25, 0.5 and 0.75 μM PV1019.

Cell culture, RNAi and cell viability assay

MCF7 cells were grown in DMEM medium with L-glutamine, supplemented with 10% fetal calf serum. OVCAR-3, OVCAR-4 and OVCAR-5 cell lines were maintained in RPMI-1640 (Lonza, Walkersville, MD) containing 5% fetal bovine serum, 2 mM L-glutamine, and no antibiotics. MCF7, OVCAR-4, OVCAR-5 and OVCAR-8 cell lines

were tested for *Mycoplasma* using the MycoAlert assay (Lonza) at the commencement of this study and found to be negative. Mouse thymocytes were isolated from wild-type or *Chk2* ^{-/-} mice by mechanical disaggregation and grown in DMEM medium with L-glutamine, supplemented with 15% fetal calf serum.

For RNAi mediated gene silencing, OVCAR-4 and OVCAR-8 cells were seeded with a complex of either negative siRNA (Allstar Negative Qiagen, Germantown, MD) or a previously validated *CHEK2* siRNA (target sequence 5'ACGCCGTCCTTTGAATAACAA 3') (Zhang et al., 2009) and oligofectamine (Invitrogen, Carlsbad, CA) at a range of concentrations (Figure 6 C and D). After 48 hours of incubation, the siRNA/lipid complex containing medium was replaced by fresh medium. Following a further 48 hours incubation, cells were assayed for cell viability using a standard MTS assay ($A_{490\text{ nm}}$) (Promega #G3580, Madison, WI).

Western blot analyses and antibodies

Whole cell lysates were prepared as previously described (Solier et al., 2008) and nuclear extract samples were made using a nuclear extract kit, following the manufacturer's instructions (Active Motif, Carlsbad, CA). Samples were subjected to SDS-PAGE and the gels were transferred to PVDF membranes. The membranes were blocked with either 5% milk (TBST) or 5% BSA (TBST), incubated overnight at 4°C with primary antibodies, washed, then incubated 1 hour with secondary antibodies; peroxidase-conjugated goat anti-mouse IgG or peroxidase-conjugated goat anti-rabbit IgG (GE healthcare). Signals were revealed by autoradiography using the Enhanced Chemiluminescence detection kit (Pierce, Rockford, IL).

The following primary antibodies were used: anti-P-Chk2 S516 (#2669, Cell Signaling, Danvers, MA), anti-Chk2 (#2662, Cell Signaling, Danvers, MA), anti-HDMX (#A300-287A, Bethyl laboratories, Montgomery, TX) and anti P-Cdc25C S216 (#9528, Cell Signaling, Danvers, MA).

Sub-G1 analysis of mouse thymocytes by flow cytometry

Three million cells were exposed to 5 Gy IR or control, in the presence or absence of 1 μ M PV1019. The cells were further incubated at 37°C for 16 hours, before fixation and permeabilization with cold (-20°C) 70% ethanol overnight, and washed with PBS. Propidium iodide (final concentration: 0.05 mg/mL) and RNase A (final concentration: 0.5 mg/mL) were added. Fluorescence intensities were determined using a FACScan flow cytometer (Becton Dickinson, Franklin Lakes, NJ) and quantified using CellQuest software (Becton Dickinson). Data was analyzed by FlowJo software (Tree Star Inc, Ashland, OR).

Drug treatment and synergy

For drug concentration-effect experiments, cells were seeded at appropriate densities (to yield ~80% confluence at time of assay) in 96-well plates and incubated at 37°C for 48 hours prior to drug addition. At 48 hours, serial dilutions of each drug (10 mM stock in DMSO) were prepared in medium. After aspirating medium from cells, 100 μ L of drug solution was added to appropriate wells. The plates were incubated at 37°C for 48 hours. Cell proliferation was assayed by adding 20 μ L MTS [3-(4, 5-dimethylthiazol-2-yl)-5-(3 carboxymethoxyphenyl)-2-(4-sulfohenyl)-2H-tetrazolium] (Promega, Madison, WI) to

each well, incubating at 37°C for 1 hour, then reading plates at 490 nm. The data was plotted using Graphpad Prism (La Jolla, CA) from raw absorbance values and was not normalized to control. The effect of single drugs alone is depicted at zero on the x-axis. Combination indices (CI) were calculated using Calcosyn software (Cambridge, UK).

Clonogenic survival assays

The human glioma cell line U251 (American Type Culture Collection, Gaithersburg, MD) was grown in RPMI 1640 containing glutamate (5 mmol/L) and 5% fetal bovine serum at 37°C in 5% CO₂ and 95% room air. A specific number of U251 cells were plated into each well of the six-well culture plates. After allowing cells to attach for 16 hours, cells were treated with PV1019 (5 μmol/L) or DMSO (vehicle control) for 1 h and then irradiated with a Pantak X-ray source at a dose rate of 2.28 Gy/min. Two hour after irradiation cells were rinsed with PBS and were replaced with fresh growth medium. The cells were further incubated for colony formation for 10 days. Colonies were fixed with methanol and stained with 0.5% crystal violet. The number of colonies containing at least 50 cells was determined and surviving fractions were calculated. Each data point was done in triplicate. Radiation survival data were fitted to a linear-quadratic model using Kaleidagraph version 4.0 (Synergy Software, Reading, PA) after normalizing for cell killing by PV1019 alone. Each point on the survival curves represents the mean surviving fraction ± SE from four independent experiments.

Kinase Profiling

Kinase profiling was performed using HotSpot technology (Reaction Biology Corp.

Malvern, PA, USA). This technology is a radioisotope-based P81 filter-binding assay. PV1019 was dissolved in pure DMSO to make a 10 mM stock. PV1019 was then diluted in pure DMSO to make a serial dilution based on the IC50 ranges. Chk2 and substrate (20 μ M CHKtide [KKKVSRSGLYRSPSPENLNRPR]) were diluted in the reaction buffer (20 mM HEPES, pH 7.5, 10 mM MgCl₂, 1 mM EGTA, 0.02% Brij35, 0.02 mg/ml BSA, 1 mM Na₃VO₄, 2 mM DTT, 1% DMSO), and then 5 nL of compound was delivered into Chk2 and substrate mixture by acoustic technology using Echo 550 (LabCyte Inc. Sunnyvale, CA). The reaction was initiated by the addition of 33P-ATP into the reaction mixture (final concentration was 10 μ M) and stopped after 2 hours incubation at room temperature. The unreacted free 33P-ATP was washed away before detection.

Results

Biochemical characterization of PV1019 (NSC 744039)

We recently reported the identification of a novel and specific Chk2 inhibitor, NSC 109555 (Jobson et al., 2007) (Figure 1A). However, NSC 109555 did not show detectable Chk2 kinase inhibition in a cellular environment. For this reason we sought to optimize the molecule. Figure 1A shows the structure of PV1019—an analogue of NSC 109555 we designed from crystal structure (Lountos et al., 2009) and selected for the present study. As part of the optimization process we desymmetrized the lead molecule (NSC 109555), retaining one of the guanadinyldiazide moieties, and coupling this via an amide bond to a 7-nitroindole substituent (shown as dotted box for PV1019) (Supplemental Materials and Methods). An *in vitro* kinase assay was used to demonstrate inhibition of Chk2 kinase function by PV1019 (NSC 744039) (Jobson et al., 2007). Figure 1B shows the dose-dependent inhibition of both Chk2 autophosphorylation and histone H1 phosphorylation. The IC_{50} for PV1019 was 138 nM, which demonstrates that PV1019 is slightly more potent than the parent compound NSC 109555 (240 nM) (Jobson et al., 2007). We also assessed whether PV1019 could inhibit Chk2-mediated phosphorylation of Cdc25C, which is a known substrate of Chk2 *in vivo* (Matsuoka et al., 1998). As Figure 1C shows, PV1019 inhibits the Chk2-dependent phosphorylation of Cdc25C in a dose-dependent fashion with an IC_{50} of 260 nM. The specificity of PV1019 for Chk2 over Chk1 was investigated, and is shown in Figure 1C. The IC_{50} for PV1019-mediated inhibition of Chk1 autophosphorylation was 55 μ M, indicating the specificity of PV1019 for Chk2 over Chk1.

To further characterize the mechanism of action of PV1019, we assessed whether PV1019 acted as a competitive inhibitor of Chk2 with respect to ATP (Figure 1D). Lineweaver-Burk analysis showed that, like the parent compound NSC 109555, PV1019 is a competitive ATP inhibitor for Chk2. Given the physiological concentration of ATP in a cellular environment, we sought to determine the impact of physiological ATP concentrations on the efficacy of PV1019. *In vitro* kinase assays were performed using 1 mM ATP. Figure 1E shows that the IC₅₀ of PV1019 was 0.57 μM under these conditions, which is 4-fold higher than the IC₅₀ determined at 10 μM ATP (Figure 1B).

Co-crystal structure of the catalytic domain of Chk2 in complex with PV1019

To elucidate the binding mode of PV1019 to Chk2, we co-crystallized the catalytic domain (residues 210-534) with the inhibitor (Supplemental Materials and Methods). The structure was refined to 2.07 Å resolution (Supplemental Table 1). The electron density maps are clearly resolved (Figure 2A) and reveal that PV1019 is located in the ATP-binding pocket of Chk2 (Figure 2B), as expected, because it is a competitive inhibitor of ATP binding (Figure 1D). Overall, the co-crystal structure is very similar to that of Chk2 in complex with ADP (r.m.s.d= 0.47 Å) and does not exhibit any significant conformational changes (Oliver et al., 2006). Electrospray mass spectrometry indicates that the purified Chk2 is phosphorylated and is thus in an active conformation (data not shown). The binding of PV1019 to Chk2 is facilitated by hydrogen bonds between the guanidinium terminus of the ligand and Glu273 on the C-α helix and the oxygen of the 7-nitro-indole of PV1019 to the backbone amide of Met304 in the hinge region (Figure 2C). There are also two important stabilizing water-mediated hydrogen bonds between

the carbonyl oxygen and the oxygen of the 7-nitro group on the ligand to the backbone carbonyl of Glu302 in the hinge and an additional water-mediated hydrogen bond between the amide nitrogen of PV1019 and the side chain carboxyl oxygen of Glu308. Additionally, several van der Waals interactions between the ATP binding pocket and PV1019 create highly complementary surfaces. The aryl and methyl moieties of the PV1019 phenyl guanidinohydrazone are involved in hydrophobic interactions with Val234, Ile251, Leu354, Ile299, and the aliphatic portions of the side chains of Lys249, Thr367, and Asp368. The 7-nitro-indole substituent on the ligand is also involved in hydrophobic interactions with Leu 226, Leu303, Gly307, Leu354, and the aliphatic portions of the side chains of Met304 and Glu308.

Kinase profiling of PV1019

To determine the selectivity of PV1019 for Chk2 kinase, *in vitro* kinase-profiling experiments were performed. The inhibitory activity of PV1019 over a panel of 53 cellular kinases indicates that PV1019 is selective toward Chk2 (Table 1). Only 13 other kinases (shown in bold text) showed some inhibition by PV1019 but their IC₅₀s were at least 75 fold greater than for Chk2. Consistent with the prior results shown in Figure 1C, PV1019 did not inhibit Chk1. These data demonstrate the specificity of PV1019 for Chk2.

Cellular inhibition of Chk2 by PV1019

To look for evidence of cellular inhibition of Chk2 by PV1019 we focused on 3 known substrates of Chk2: Chk2 itself (autophosphorylation), HDMX and Cdc25C. An

abbreviated molecular interaction map of these phosphorylations is depicted in Figure 3A. The dose-dependent effect of PV1019 on IR-induced Chk2 autophosphorylation at Ser516 in OVCAR-4 cells is shown in Figure 3B. The IC_{50} was 5 μ M. Total Chk2 levels were also measured in these experiments and at lower concentrations of PV1019 showing inhibition of Chk2 autophosphorylation, there was no change in level of Chk2. Interestingly, at higher concentrations of PV1019, there was a decrease in the level of Chk2 total protein. In addition, we assessed the degree of Chk2 inhibition using a previously reported Chk2 inhibitor, 2-arylbenzimidazole (ABI), Figure 3C. ABI showed a comparable level of Chk2 inhibition at 25 μ M compared to that seen with PV1019. To further investigate the effect of PV1019 on Chk2 kinase inhibition, we used OVCAR-5 cells (which were used for synergy studies later). We assessed two different protocols for topotecan (TPT) and PV1019 exposure, co-incubation (figure 3C) and pretreatment with TPT, followed by PV1019 treatment (figure 3D). The level of Chk2 autophosphorylation (S516) was measured by Western blotting. In both cases PV1019 was shown to inhibit the TPT-induced Chk2 autophosphorylation. Indeed, a concentration as low as 1 μ M of PV1019 was able to inhibit the TPT-induced Chk2 autophosphorylation (IC_{50} was 2.8 μ M Figure 3 C).

It has been reported that in response to DNA damage, Chk2 phosphorylates HDMX on Ser367, which leads to HDMX degradation (Figure 3A). This degradation can be abrogated by the Chk2 inhibitor, 2-arylbenzimidazole (ABI) (Pereg et al., 2006). Figure 3E shows that exposure of MCF7 cells to 1 μ M TPT for 4 hours led to the expected decrease in the cellular level of HDMX. Co-incubating the cells with PV1019 decreased the level of HDMX degradation induced by TPT exposure. Abrogation of HDMX

degradation after TPT treatment by PV1019 provides evidence of PV1019 inhibiting Chk2 kinase activity.

We also observed the level of IR-induced Ser516 phosphorylation was significantly decreased when MCF7 cells were exposed to PV1019 at 10 or 25 μM ($\text{IC}_{50} < 10 \mu\text{M}$; Figure 3F). Similarly, under identical assay conditions, the level of IR-induced Cdc25C phosphorylation on Ser216 was decreased by more than 50% in the presence of 10 μM PV1019. These data provide convergent evidence for cellular inhibition of Chk2 by PV1019.

Abrogation of IR-induced apoptosis in mouse thymocytes by PV1019

Chk2 activation is known to induce apoptosis in thymocytes by activating p53 (Hirao et al., 2000). To further investigate the inhibitory effect of PV1019 on Chk2, we studied IR-induced apoptosis in normal mouse thymocytes. Previously, Chk2 $-/-$ mouse thymocytes have been shown to be resistant to IR (Hirao et al., 2000). In addition, the recently reported Chk2 inhibitor VRX0466617 was shown to abrogate IR-induced apoptosis in normal mouse thymocytes (Carlessi et al., 2007). We performed experiments with PV1019 to test whether we could emulate this phenomenon using flow cytometry to measure sub-G1 (apoptotic) cells. Figure 4A shows the effect of 5 Gy IR on wild-type mouse thymocytes. IR exposure produced a large sub-G1 fraction of cells (71.9%) compared to untreated control cells (11.5%). Pretreatment of normal thymocytes with PV1019, showed a decrease in the sub-G1 fraction (56%). Furthermore, in Chk2 $-/-$ cells, exposure to 5 Gy IR and incubation for 16 hours showed a comparable reduction of the sub-G1 cells from 71.9% (control thymocytes) to 52.2% (Chk2 $-/-$ thymocytes) (Figure

4B). This result corroborates the observed effect of PV1019 decreasing the number of sub-G1 cells in Chk2 wild-type cells following exposure to IR (see Figure 4A). These data provide further evidence for the inhibition of cellular Chk2 kinase by PV1019.

PV1019 potentiates the activity of chemotherapeutic agents in human tumor cells

To test whether Chk2 inhibition could sensitize the cells to chemotherapeutic agents, we investigated whether PV1019 could enhance the effect of topoisomerase I inhibitors and ionizing radiations in human tumor cells. We used two different ovarian cancer cell lines from the NCI60 to evaluate the effect of PV1019. Figure 5A shows that concentrations of 3 and 25 μM PV1019 augmented the growth inhibitory effect TPT, decreasing the IC_{50} up to 5.7-fold (25 μM PV1019) in OVCAR-5 following a 48 hour exposure period. The IC_{50} of PV1019 alone was 58 μM . To confirm PV1019 synergized the effect of TPT, we calculated combination indices (CI) with a range of concentrations of PV1019 and TPT using the program Calcosyn. Figure 5B shows synergy as the combination indices were below one (Chou and Talalay, 1984). We also examined the effect of the combination of PV1019 and TPT in OVCAR-4 cells (Figure 5C). A full growth inhibitory response was not achieved with increasing concentrations of TPT alone, although an IC_{50} was attained. However, PV1019 increased the maximum growth inhibitory effect of TPT, while the IC_{50} of PV1019 alone was 18.7 μM . Combination indices were calculated using the Calcosyn and the values tabulated in Figure 5D. Again, synergism was observed in the OVCAR-4 cells. We also tested whether the growth inhibitory effect of the parental compound camptothecin (CPT) could also be augmented. Figure 5E shows that in

OVCAR-4, similar to TPT, PV1019 was able to enhance the maximum growth inhibitory of CPT.

We next determined the effects of PV1019 on tumor cell (U251) radiosensitivity. Five μM PV1019 provided approximately 33% toxicity with 3 hours incubation in U251 cells as a single agent. Treatment of U251 cells with 5 μM PV1019 (1 hour pre- and 2 hours post-IR) radiosensitized U251 cells with a dose enhancement factor (DEF) 1.4 (Figure 5F). Under these conditions the cell cycle profile of PV1019 did not change (data not shown).

Taken together, these results demonstrate that PV1019 potentiates the cell killing effect of topoisomerase I inhibitors (TPT and CPT) and IR in several cancer cell lines.

Effect of Chk2 inhibition or down-regulation of Chk2 on growth of tumor cells lines.

It has previously been reported that HCT15 cells are functionally deficient for Chk2 as they express a mutant form of Chk2 that is rapidly degraded (Falck et al., 2001). To further investigate the selectivity of PV1019 for Chk2 kinase, we investigated the sensitivity of HCT15 cells to PV1019. Since HCT15 are part of the panel of colon carcinoma cell lines in the NCI60 cell panel (<http://discover.nci.nih.gov/cellminer/>), we compared the antiproliferative activity of PV1019 across the colon and ovarian cell lines from the NCI-60. Figures 6 A and B show growth inhibitory responses. HCT15 cells, which are known to be deficient for Chk2 (Figure 6C), showed resistance to PV1019 when compared to the other colon cell lines. In addition, we observed that SK-OV3 cells also showed a lack of PV1019-mediated growth inhibition. Western blotting showed almost undetectable levels of Chk2 in SK-OV3 (Figure 6D). In contrast, KM12,

OVCAR-3, OVCAR-4 and OVCAR-8, which were among the most sensitive to PV1019 (Figures 6A and B), expressed high levels of Chk2 (Figures 6C and D). These data are consistent with the possibility that the antiproliferative effects mediated by PV1019 are related to Chk2 inhibition.

To confirm the antiproliferative effect of Chk2 inhibition in human tumor cells, we investigated the effect of RNAi mediated gene silencing of *CHEK2* in two different ovarian cell lines, OVCAR-4 and OVCAR-8 that express high levels of Chk2 (Figures 6 C and D). The *CHEK2* RNAi used has been previously validated and reported (Zhang et al., 2009). In both cell lines down-regulation of *CHEK2* caused a growth inhibitory effect when compared to RNAi control (Figures 6E and F). An additional *CHEK2* siRNA was also used in OVCAR-8 and showed a similar inhibitory effect (data not shown). These data provide evidence that Chk2 inhibition can produce antiproliferative activity in cancer cells that express high endogenous Chk2 levels.

Discussion

Recently we identified and characterized a Chk2 inhibitor, NSC 109555, with a novel chemotype (Jobson et al., 2007) and co-crystallized NSC 109555 with the catalytic domain of Chk2 (Lountos et al., 2009). Seeking to improve the cellular activity of NSC 109555 while maintaining selectivity for Chk2, a new analog PV1019 (NSC 744039) was synthesized. (Figure 1A). In the present study, we report that PV1019 is an ATP-competitive inhibitor (Figure 1D) that exhibits cellular Chk2 inhibition while exhibiting higher potency than NSC 109555 while retaining specificity for Chk2 (IC_{50} of 24-260 nM, see Figure 1 and Table 1).

Because the IC_{50} values determined in the *in vitro* kinase assays and cellular assays (Figures 1 and 3, respectively) showed around a 100-fold difference, we examined the activity of PV1019 in the presence of physiological concentrations of ATP in order to better relate the relationship between *in vitro* kinase and cellular inhibition results. As expected, a more physiological concentration of ATP, 1 mM, decreased the activity of PV1019, which may explain the higher (low micro-molar) concentration required to inhibit Chk2 kinase in cells. Also, we cannot exclude the impact of drug uptake and any metabolism/degradation of PV1019 in the cellular studies.

Selectivity for Chk2 kinase was maintained with PV1019 as demonstrated via a kinase panel profiling experiment. Importantly, as with NSC 109555, PV1019 was markedly more selective for Chk2 than Chk1 (655-fold) (Table 1). Other agents that are under clinical evaluation do not elicit this specificity for Chk2 over Chk1. Thus, PV1019 may

provide a novel chemotype for developing new therapeutic agents. A number of the kinases that showed some inhibition by PV1019 (DAPK1, Chk1, PHKg2, PIM1, RSK1 and RSK2) (highlighted in gray in Table 1) are part of the same phylogenetic tree in the human kinome, CAMK (Manning et al., 2002). This observation demonstrates the potential difficulty of developing highly specific kinase inhibitors. However, in the case of PV1019, at least a 75-fold selectivity was observed for Chk2 over the other kinases tested.

In this study, we have demonstrated that PV1019 is capable of inhibiting the kinase activity of Chk2 in a cellular environment. We have shown inhibition of Chk2 and abrogation of downstream substrate phosphorylation/function for Cdc25C and HDMX by PV1019 (see Figures 3 B, C and D). In addition, the level of Chk2-dependent IR-induced apoptosis was decreased by PV1019 in normal mouse thymocytes (Figure 4A), which is in accordance with another Chk2 inhibitor, VRX0466617 (Carlessi et al., 2007). Collectively these cellular assays demonstrate inhibition of Chk2 kinase activity by PV1019 in cells. We also found a correlation between the antiproliferative activity of PV1019 in the ovarian and colon cell lines from the NCI60 cell screen from the DTP and the levels of Chk2 expression.

Chk2 inhibitors have been proposed as chemotherapeutic agents in combination with cytotoxic agents [for review see (Pommier et al., 2005; Antoni et al., 2007)]. This hypothesis has not been clearly demonstrated when using pharmacological inhibition of Chk2 combined with cytotoxic agents. Indeed, a recently reported Chk2 inhibitor,

VRX0466617, did not show synergy with a number of anti-cancer agents (Carlessi et al., 2007). However, the authors could not exclude the possibility that VRX0466617 inhibits Aurora A kinase. Our studies utilized OVCAR-4 and OVCAR-5 ovarian human tumor cells to test this hypothesis with cytotoxic agents. We have demonstrated synergy of cytotoxic agents in combination with PV1019 in those cell lines. Likewise, PV1019 was shown to enhance the cell killing of radiation in the human brain tumor cell line, U251. Together, our data suggest the use of a Chk2 inhibitor in combination with topoisomerase I inhibitor chemotherapy or radiation. In addition to the use of Chk2 inhibitors with either cytotoxic agents or radiation, we have also shown the potential of using PV1019 as a single agent. Consistently, the two Chk2-deficient cell lines, HCT15 (Falck et al., 2001) and SK-OV3 are not affected by PV1019 (see Figure 6) and down-regulation of Chk2 leads to growth inhibition in two of the ovarian cell lines with the highest Chk2 expression. These results suggest the potential activity of Chk2 inhibitors as single agents in cancer cells with high Chk2 expression.

The determination of the crystal structure of the catalytic domain of Chk2 in complex with PV1019 provided a detailed view of the molecular interactions between the compound and the ATP-binding pocket and enabled us to compare and contrast its mode of binding with that of the lead compound NSC 109555 (Figure 2D). PV1019 retains many of the same interactions with the ATP-binding pocket that were observed in the complex with NSC 109555 (Lountos et al., 2009), including the hydrogen bond with Glu273 and the hydrophobic interactions between the aryl and methyl moieties of the phenyl guanidinohydrazone and the ATP binding pocket. The methyl group of PV1019

also projects towards a hydrophobic pocket in the enzyme as previously observed in the Chk2/NSC 109555 complex. This hydrophobic pocket is of considerable interest because it may present an opportunity to modulate the potency and specificity of Chk2 inhibitors; its shape, accessibility and degree of hydrophobicity vary among kinases (Toledo et al., 1999; Scapin, 2002; Lountos et al., 2009). Accordingly, functional replacements for the methyl group of PV1019, such as branched and cyclic alkanes, may fill this pocket and further improve potency and specificity. Due to the incorporation of the 7-nitro-indole substituent, PV1019 picks up new interactions with the ATP-binding pocket which likely account for its increased potency over the parent compound NSC 109555 (Lountos et al., 2009). The 7- nitro group incorporates two new interactions, a water-mediated hydrogen bond to the backbone carbonyl oxygen of Glu302 and a hydrogen bond to the backbone amide of Met304 in the hinge and the amide nitrogen of PV1019 also picks up a water-mediated hydrogen bond to the carboxyl side chain oxygen of Glu308. The indole ring is also involved in favorable van der Waals interactions with several hydrophobic residues in the ATP-binding pocket. Taken together, the conservation of the molecular interactions with the phenyl guanidinohydrazone and the new molecular interactions with the 7-nitro-indole group likely contribute to the increased potency of PV1019. These observations will facilitate the further development of PV1019 derivatives.

In summary, we have developed a potent and specific inhibitor of Chk2 kinase. We have shown inhibition in a cellular context and demonstrated that the inhibitor synergizes two cytotoxic agents and radiation in human tumor cell lines. These data provide evidence to consider this inhibitor for preclinical development in animal models.

Acknowledgements:

We thank Dr. Noboru (National center for geriatrics and ontology, Aichi, Japan) and Dr. Liu Cao (National heart, lung and blood institute, NIH) for providing and isolating wild type and *Chk2* ^{-/-} thymocytes. Qiagen Inc. supplied *CHEK2* siRNA used in this study to the NCI as part of a Collaborative Research Agreement. We thank Tamara Jones for technical assistance.

References

- Ahn J and Prives C (2002) Checkpoint kinase 2 (Chk2) monomers or dimers phosphorylate Cdc25C after DNA damage regardless of threonine 68 phosphorylation. *J Biol Chem* **277**:48418-48426.
- Ahn JY, Schwarz JK, Piwnica-Worms H and Canman CE (2000) Threonine 68 phosphorylation by ataxia telangiectasia mutated is required for efficient activation of Chk2 in response to ionizing radiation. *Cancer Res* **60**:5934-5936.
- Antoni L, Sodha N, Collins I and Garrett MD (2007) CHK2 kinase: cancer susceptibility and cancer therapy - two sides of the same coin? *Nat Rev Cancer* **7**:925-936.
- Arienti KL, Brunmark A, Axe FU, McClure K, Lee A, Blevitt J, Neff DK, Huang L, Crawford S, Pandit CR, Karlsson L and Breitenbucher JG (2005) Checkpoint kinase inhibitors: SAR and radioprotective properties of a series of 2-arylbenzimidazoles. *J Med Chem* **48**:1873-1885.
- Ariumi Y, Kuroki M, Dansako H, Abe K, Ikeda M, Wakita T and Kato N (2008) The DNA damage sensors ataxia-telangiectasia mutated kinase and checkpoint kinase 2 are required for hepatitis C virus RNA replication. *J Virol* **82**:9639-9646.
- Ashwell S, Janetka JW and Zabludoff S (2008) Keeping checkpoint kinases in line: new selective inhibitors in clinical trials. *Expert Opin Investig Drugs* **17**:1331-1340.
- Bartkova J, Horejsi Z, Koed K, Kramer A, Tort F, Zieger K, Guldborg P, Sehested M, Nesland JM, Lukas C, Orntoft T, Lukas J and Bartek J (2005) DNA damage response as a candidate anti-cancer barrier in early human tumorigenesis. *Nature* **434**:864-870.

- Carlessi L, Buscemi G, Larson G, Hong Z, Wu JZ and Delia D (2007) Biochemical and cellular characterization of VRX0466617, a novel and selective inhibitor for the checkpoint kinase Chk2. *Mol Cancer Ther* **6**:935-944.
- Castedo M, Perfettini JL, Roumier T, Yakushijin K, Horne D, Medema R and Kroemer G (2004) The cell cycle checkpoint kinase Chk2 is a negative regulator of mitotic catastrophe. *Oncogene* **23**:4353-4361.
- Chabalier-Taste C, Racca C, Dozier C and Larminat F (2008) BRCA1 is regulated by Chk2 in response to spindle damage. *Biochim Biophys Acta*.
- Chou TC and Talalay P (1984) Quantitative analysis of dose-effect relationships: the combined effects of multiple drugs or enzyme inhibitors. *Adv Enzyme Regul* **22**:27-55.
- Curman D, Cinel B, Williams DE, Rundle N, Block WD, Goodarzi AA, Hutchins JR, Clarke PR, Zhou BB, Lees-Miller SP, Andersen RJ and Roberge M (2001) Inhibition of the G2 DNA damage checkpoint and of protein kinases Chk1 and Chk2 by the marine sponge alkaloid debromohymenialdisine. *J Biol Chem* **276**:17914-17919.
- Falck J, Lukas C, Protopopova M, Lukas J, Selivanova G and Bartek J (2001) Functional impact of concomitant versus alternative defects in the Chk2-p53 tumour suppressor pathway. *Oncogene* **20**:5503-5510.
- Ghosh JC, Dohi T, Raskett CM, Kowalik TF and Altieri DC (2006) Activated checkpoint kinase 2 provides a survival signal for tumor cells. *Cancer Res* **66**:11576-11579.
- Gorgoulis VG, Vassiliou LV, Karakaidos P, Zacharatos P, Kotsinas A, Liloglou T, Venere M, Ditullio RA, Jr., Kastriakis NG, Levy B, Kletsas D, Yoneta A,

- Herlyn M, Kittas C and Halazonetis TD (2005) Activation of the DNA damage checkpoint and genomic instability in human precancerous lesions. *Nature* **434**:907-913.
- Hirao A, Kong YY, Matsuoka S, Wakeham A, Ruland J, Yoshida H, Liu D, Elledge SJ and Mak TW (2000) DNA damage-induced activation of p53 by the checkpoint kinase Chk2. *Science* **287**:1824-1827.
- Jobson AG, Cardellina JH, 2nd, Scudiero D, Kondapaka S, Zhang H, Kim H, Shoemaker R and Pommier Y (2007) Identification of a Bis-guanylhydrazone [4,4'-Diacetyldiphenylurea-bis(guanylhydrazone); NSC 109555] as a novel chemotype for inhibition of Chk2 kinase. *Mol Pharmacol* **72**:876-884.
- Kohn KW (1999) Molecular interaction map of the mammalian cell cycle control and DNA repair systems. *Mol Biol Cell* **10**:2703-2734.
- Lapenna S and Giordano A (2009) Cell cycle kinases as therapeutic targets for cancer. *Nat Rev Drug Discov* **8**:547-566.
- Larson G, Yan S, Chen H, Rong F, Hong Z and Wu JZ (2007) Identification of novel, selective and potent Chk2 inhibitors. *Bioorg Med Chem Lett* **17**:172-175.
- Lau A, Swinbank KM, Ahmed PS, Taylor DL, Jackson SP, Smith GC and O'Connor MJ (2005) Suppression of HIV-1 infection by a small molecule inhibitor of the ATM kinase. *Nat Cell Biol* **7**:493-500.
- Lountos GT, Tropea JE, Zhang D, Jobson AG, Pommier Y, Shoemaker RH and Waugh DS (2009) Crystal structure of checkpoint kinase 2 in complex with NSC 109555, a potent and selective inhibitor. *Protein Science*:92-100.

- Manning G, Whyte DB, Martinez R, Hunter T and Sudarsanam S (2002) The protein kinase complement of the human genome. *Science* **298**:1912-1934.
- Matsuoka S, Huang M and Elledge SJ (1998) Linkage of ATM to cell cycle regulation by the Chk2 protein kinase. *Science* **282**:1893-1897.
- Matthews DJ, Yakes FM, Chen J, Tadano M, Bornheim L, Clary DO, Tai A, Wagner JM, Miller N, Kim YD, Robertson S, Murray L and Karnitz LM (2007) Pharmacological abrogation of S-phase checkpoint enhances the anti-tumor activity of gemcitabine in vivo. *Cell Cycle* **6**:104-110.
- Oliver AW, Paul A, Boxall KJ, Barrie SE, Aherne GW, Garrett MD, Mitnacht S and Pearl LH (2006) Trans-activation of the DNA-damage signalling protein kinase Chk2 by T-loop exchange. *Embo J* **25**:3179-3190.
- Pereg Y, Lam S, Teunisse A, Biton S, Meulmeester E, Mittelman L, Buscemi G, Okamoto K, Taya Y, Shiloh Y and Jochemsen AG (2006) Differential roles of ATM- and Chk2-mediated phosphorylations of Hdmx in response to DNA damage. *Mol Cell Biol* **26**:6819-6831.
- Pommier Y, Sordet O, Rao VA, Zhang H and Kohn KW (2005) Targeting chk2 kinase: molecular interaction maps and therapeutic rationale. *Curr Pharm Des* **11**:2855-2872.
- Pommier Y, Weinstein JN, Aladjem MI and Kohn KW (2006) Chk2 molecular interaction map and rationale for Chk2 inhibitors. *Clin Cancer Res* **12**:2657-2661.
- Scapin G (2002) Structural biology in drug design: selective protein kinase inhibitors. *Drug Discov Today* **7**:601-611.

- Sharma V and Tepe JJ (2004) Potent inhibition of checkpoint kinase activity by a hymenialdisine-derived indoloazepine. *Bioorg Med Chem Lett* **14**:4319-4321.
- Solier S, Sordet O, Kohn KW and Pommier Y (2008) Death Receptor-Induced Activation of the Chk2- and Histone H2AX-associated DNA Damage Response Pathways. *Mol Cell Biol*.
- Takai H, Naka K, Okada Y, Watanabe M, Harada N, Saito S, Anderson CW, Appella E, Nakanishi M, Suzuki H, Nagashima K, Sawa H, Ikeda K and Motoyama N (2002) Chk2-deficient mice exhibit radioresistance and defective p53-mediated transcription. *Embo J* **21**:5195-5205.
- Toledo LM, Lydon NB and Elbaum D (1999) The structure-based design of ATP-site directed protein kinase inhibitors. *Curr Med Chem* **6**:775-805.
- Vakifahmetoglu H, Olsson M, Tamm C, Heidari N, Orrenius S and Zhivotovsky B (2008) DNA damage induces two distinct modes of cell death in ovarian carcinomas. *Cell Death Differ* **15**:555-566.
- Wu X and Chen J (2003) Autophosphorylation of checkpoint kinase 2 at serine 516 is required for radiation-induced apoptosis. *J Biol Chem* **278**:36163-36168.
- Yu Q, La Rose J, Zhang H, Takemura H, Kohn KW and Pommier Y (2002) UCN-01 inhibits p53 up-regulation and abrogates gamma-radiation-induced G(2)-M checkpoint independently of p53 by targeting both of the checkpoint kinases, Chk2 and Chk1. *Cancer Res* **62**:5743-5748.
- Yu Q, Rose JH, Zhang H and Pommier Y (2001) Antisense inhibition of Chk2/hCds1 expression attenuates DNA damage-induced S and G2 checkpoints and enhances apoptotic activity in HEK-293 cells. *FEBS Lett* **505**:7-12.

Zabludoff SD, Deng C, Grondine MR, Sheehy AM, Ashwell S, Caleb BL, Green S, Haye HR, Horn CL, Janetka JW, Liu D, Mouchet E, Ready S, Rosenthal JL, Queva C, Schwartz GK, Taylor KJ, Tse AN, Walker GE and White AM (2008) AZD7762, a novel checkpoint kinase inhibitor, drives checkpoint abrogation and potentiates DNA-targeted therapies. *Mol Cancer Ther* **7**:2955-2966.

Zhang YW, Jones TL, Martin SE, Caplen NJ and Pommier Y (2009) Implication of Checkpoint Kinase-dependent Up-regulation of Ribonucleotide Reductase R2 in DNA Damage Response. *J Biol Chem* **284**:18085-18095.

Footnotes

This research was supported by the Intramural Research Program (Center for Cancer Research, NCI) of the NIH. X-ray diffraction data were collected at the Southeast Regional Collaborative Access Team (SER-CAT) beamlines 22-ID and 22-BM at the Advanced Photon Source, Argonne National Laboratory. Supporting institutions may be found at <http://www.ser-cat.org/members.html>. Use of the Advanced Photon Source was supported by the U.S. Department of Energy, Office of Science, Office of Basic Energy Sciences, under contract no. W-31-109-Eng-38.

Legends for Figures

Figure 1. PV1019 is a selective and potent inhibitor of Chk2 kinase *in vitro*. **A**, Structures of NSC 109555 (Jobson et al., 2007) and PV1019. The differences are shown by dotted boxes. **B**, Chk2 was incubated with histone H1 and varying concentrations of either NSC 109555 or PV1019 for the indicated times in an *in vitro* kinase assay. Representative gel of a Chk2 inhibitor experiment for PV1019. **C**, Effect of increasing concentrations of PV1019 on Chk2 and GST-Cdc25C (upper) and on Chk1 and histone H1 phosphorylation (lower). Representative gels are shown. **D**, Competitive inhibition of Chk2 by PV1019 with respect to ATP. The data are plotted using double reciprocal (Lineweaver-Burk) plots. **E**, Effect of 1 mM ATP on PV1019-mediated inhibition of Chk2. Chk2 was incubated with histone H1 and varying concentrations of PV1019 in an *in vitro* kinase assay containing 1 mM ATP. The percent inhibition of Chk2-mediated histone H1 phosphorylation is represented graphically.

Figure 2. Co-crystal structure of PV1019 bound in the ATP-binding pocket of the catalytic domain of Chk2. **A**, Coordinates of PV1019 superimposed on the final $2F_o - F_c$ electron density maps at 2.07 Å resolution contoured at the 1σ level. Atoms are colored as carbon (gray), nitrogen (blue), and oxygen (red). **B**, Crystal structure of the catalytic domain of Chk2 in complex with PV1019. The protein is illustrated in ribbons and the inhibitor is shown in space-filling spheres with carbon (gray), nitrogen (blue), and oxygen (red). **C**, LIGPLOT schematic of the molecular interactions of PV1019 with the ATP-binding pocket of Chk2. Residues involved in hydrogen bonding to the ligand are

illustrated in stick-format, water molecules are shown as cyan spheres, and hydrogen bonds are shown as green dashes. The “half-suns” represent hydrophobic interactions between the protein and ligand. **D**, Superposition of the Chk2-PV1019 (red sticks, PDB code: 2w7x) complex with Chk2-NSC 109555 (green sticks, PDB code: 2w0j) and Chk2-ADP (cyan sticks, PDB code: 2cn5) complexes illustrating the binding conformations of the two inhibitors and ADP. The protein side chain coordinates are from the Chk2-PV1019 structure with carbon (gray), nitrogen (blue), oxygen (red), and sulfur (yellow).

Figure 3. Evidence for cellular inhibition of Chk2 kinase by PV1019. **A**, Abbreviated molecular interaction map depicting the phosphorylations of Chk2, Cdc25C and HDMX following Chk2 activation. The conventions used for the interactions (Kohn, 1999) are as follows: the line with an open circle indicates enzymatic stimulation and phosphorylation, the line with an open arrow-head indicates general stimulation and the open circle with a line crossing through indicates degradation. For details of the molecular interaction map for Chk2 see (Pommier et al., 2006). **B**, OVCAR-4 cells were exposed to 10 Gy IR followed by a 1 hour incubation in the presence or absence of PV1019 or 2-arylbenzimidazole (ABI) (pre-incubated for 1 hour). The levels of Chk2 phosphorylated on S516 and total Chk2 were detected by Western blotting. Actin was used as loading control. **C**, OVCAR-5 cells were exposed to PV1019 and TPT (or control) for 1 hour. The levels of Chk2 phosphorylated on S516 were detected by Western blotting. Actin was used as loading control. **D**, OVCAR-5 cells were pretreated with TPT for 1 hour, the drug was washed off and the cells were exposed to PV1019 (or control) for an additional hour. The levels of Chk2 phosphorylated on S516 were detected by Western blotting.

Actin was used as loading control. **E**, MCF7 cells were exposed to either 1 μ M TPT for 4 hours or 10 Gy IR followed by a 4 hour incubation in the presence or absence of PV1019 (pre-incubated for 2.5 hours). Western blotting using anti-HDMX antibodies was performed to measure the levels of HDMX. Representative gels are depicted and the quantified levels of HDMX are shown in the graphs below. **F**, MCF7 cells were exposed to 10 Gy IR followed by a 1 hour incubation in the presence or absence of PV1019 (pre-incubated for 2.5 hours). The levels of Chk2 phosphorylated on S516 were detected by Western blotting (upper panel). The levels of Cdc25C phosphorylated on S216 were detected by Western blotting (lower panel). Actin was used as a loading control for each experiment.

Figure 4. Abrogation of IR-induced apoptosis by PV1019 in mouse thymocytes. Wild type (**A**) or Chk2 $-/-$ (**B**) mouse thymocytes were isolated and exposed to 5 Gy IR (or control) and incubated for 16 hours in the presence or absence of 1 μ M PV1019 (pre-incubated for 1 hour). Cells were stained with PI and analyzed by flow cytometry. Representative graphs show the number of cells in G1 and sub-G1 cell cycle phases. The percentage of cells in either the G1 or sub-G1 cell cycle phase is shown.

Figure 5. PV1019 synergistically inhibits cellular proliferation with topoisomerase I inhibitors in ovarian human tumor cell lines and synergizes the effect of radiation in the brain tumor cell line, U251. The indicated cell lines OVCAR-5 (**A**) and OVCAR-4 (**C and E**) cells were incubated with varying concentrations of TPT (**A and C**) and CPT (**E**) alone, or co-incubated with varying concentrations of TPT or CPT and fixed

concentrations of PV1019 for 48 hours in 96 well plates. MTS was added to the plates and the absorbance at 495 nm was measured. Combination indices (CI) for **A** and **C** were calculated using CalcuSyn software and the values tabulated (**B** and **D**, respectively). **F**, U251 cells were seeded in six-well tissue culture plates and radiation was delivered 16 hours later. U251 cells were treated with 5 μ M PV1019 1 hour prior to different dose (0, 2, 4, 6, 8 Gy) of ionizing radiation (IR). All cells including DMSO vehicle control were rinsed with PBS and cultures were replaced with fresh growth medium 2 hours following IR. The number of colonies were determined 10 days later, and survival curves were generated after normalizing for cell killing by PV1019 alone. Dose enhancing factor (DEF) was calculated at a surviving fraction of 0.1. The average plating efficiency (PE) with 5 μ M PV1019 alone was approximately 67%. Data represents mean \pm SE from four independent experiments in triplicate.

Figure 6. PV1019 causes growth inhibition in a panel of colon and ovarian human tumor cell lines that mimics the effect of Chk2 RNAi in ovarian human tumor cells.

A, The human colon carcinoma cell lines from the NCI-60 were incubated with varying concentrations of PV1019 for 48 hours. The cells were subjected to the sulphorhodamine (SRB) assay and GI_{50} values were determined. **B**, The human tumor ovarian cell lines from the NCI-60 were incubated with varying concentrations of PV1019 for 48 hours. The cells were subjected to the sulphorhodamine B (SRB) assay and GI_{50} values were determined. **C-D**, Chk2 protein levels measured by Western blot in the colon (**C**) and ovarian (**D**) cell lines from the NCI Developmental Therapeutics Program (DTP) screen. **E**, OVCAR-4 cells were transfected with either control siRNA or *CHEK2* siRNA and

incubated for 96 hours in 96 well plates. MTS was added to the plates and the absorbance at 495 nm was measured. Representative experiments are shown. **F**, OVCAR-8 cells were transfected with either control siRNA or *CHEK2* siRNA and incubated for 96 hours in 96 well plates. MTS was added to the plates and the absorbance at 495 nm was measured. Representative experiments are shown.

Table 1. Kinase profiling data for PV1019^A

Kinase	IC₅₀ (nM)	Kinase	IC₅₀ (nM)
	PV 1019		PV 1019
ABL1	>20,000	IR	>20,000
ALK	>20,000	IRAK4	>20,000
AKT1 (dPH, S473D)	10,900	JAK2	>20,000
Aurora A	>20,000	JAK3	>20,000
BTK	>20,000	KDR/VEGFR2	>20,000
CAMKIIb	>20,000	LCK	>20,000
CDK1/cyclinB	1,835	Lyn	>20,000
CDK2/cyclinA	>20,000	MINK	2,261
CHK1	15,730	MST2 /STK3	>20,000
CHK2	24	P38 α /MAPK14	>20,000
c-MET	>20,000	PAK2	8,579
c-Src	>20,000	PDGFR α	>20,000
DAPK1	8,743	PHKg2	5,707
EGFR	>20,000	PIM1	4,749
EphA3	>20,000	PKA	9,469
EphB4	>20,000	PKC α	>20,000
ErbB4 /HER4	>20,000	PLK2	>20,000
ERK1	>20,000	RET	>20,000
ERK2/MAPK2 /P42MAPK	>20,000	ROCK-I	9,405

FGFR1	>20,000	RSK1	10,970
FGFR2	>20,000	RSK2	3,613
FGFR3	>20,000	Syk	>20,000
FLT1 /VEGFR1	>20,000	TAK1-TAB1	>20,000
FLT3	>20,000	TIE2	>20,000
FLT4	>20,000	TRKA/NTRK1	>20,000
GSK3 β	>20,000	ZAP70	>20,000
HIPK1	10,780		

^A Experiments were performed by Reaction Biology Corporation (<http://www.reactionbiology.com/>) using a radioactive assay method. Ten concentration curves were run with 10 μ M ATP. Kinases showing some inhibition are in bold and evolutionarily related kinases (Manning et al., 2002) are highlighted in gray.

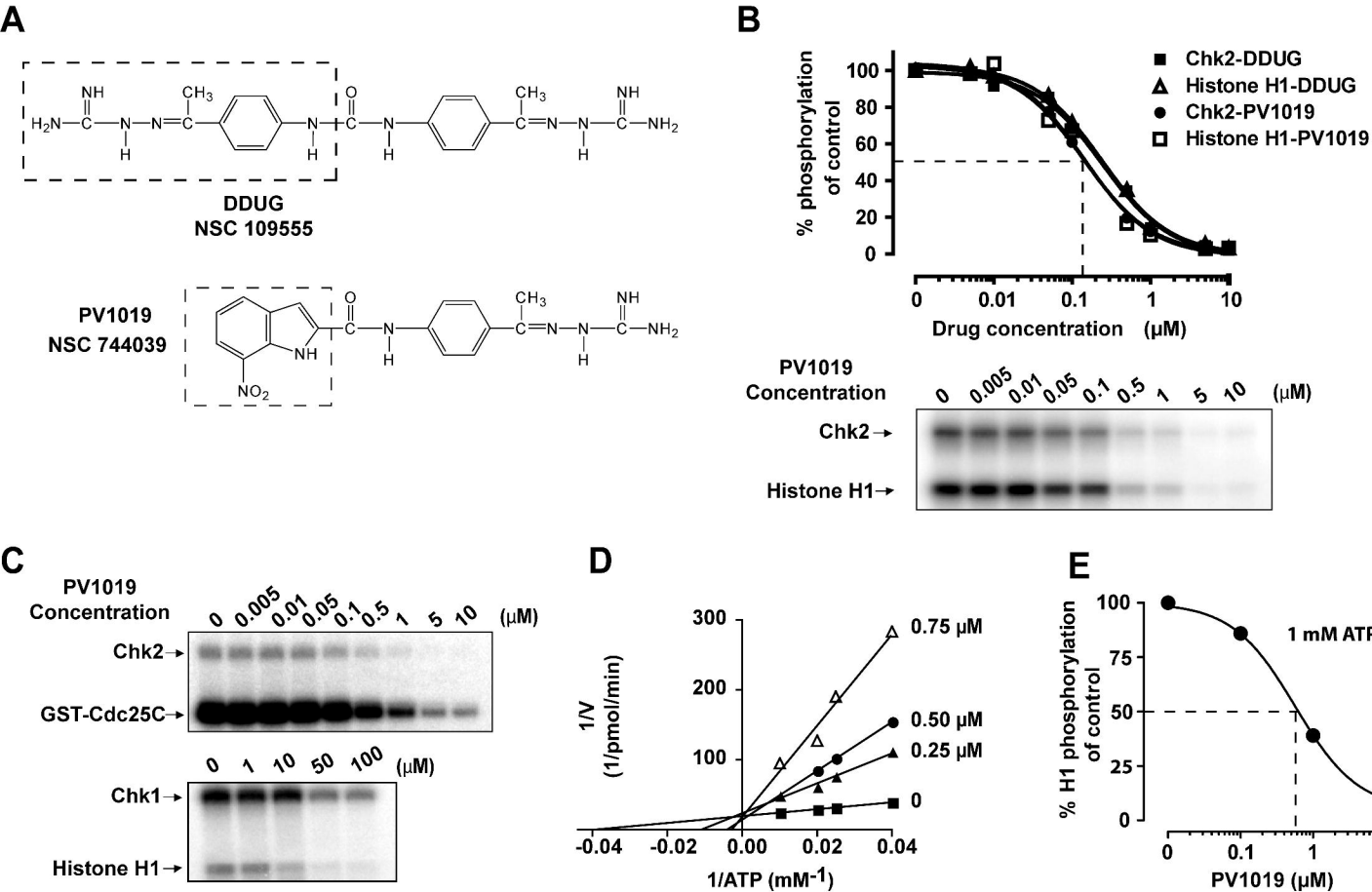


Figure 1

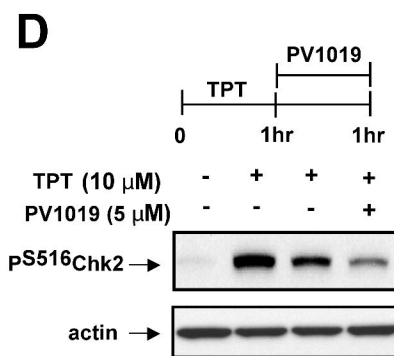
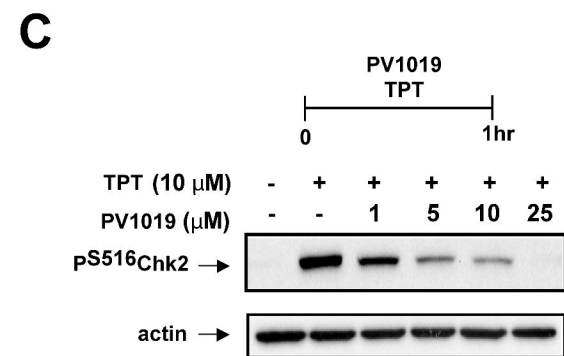
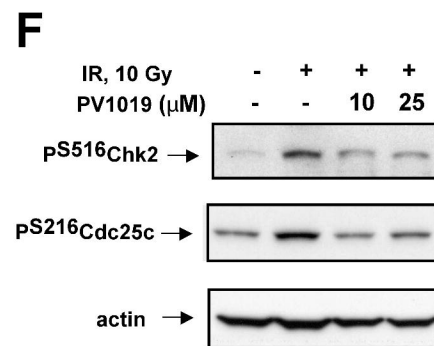
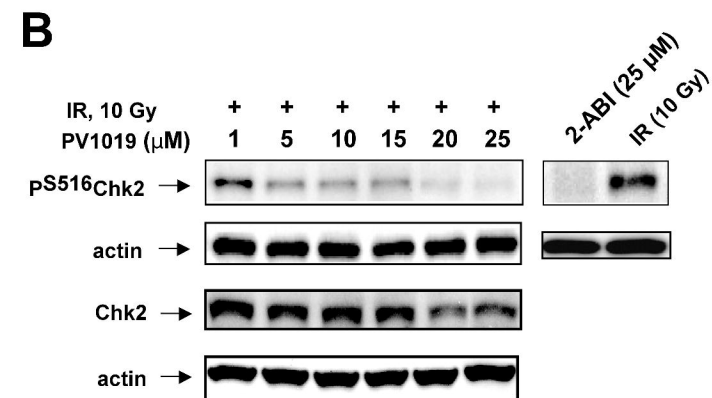
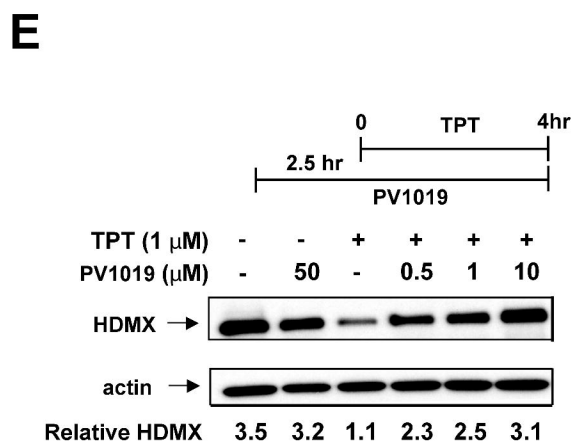
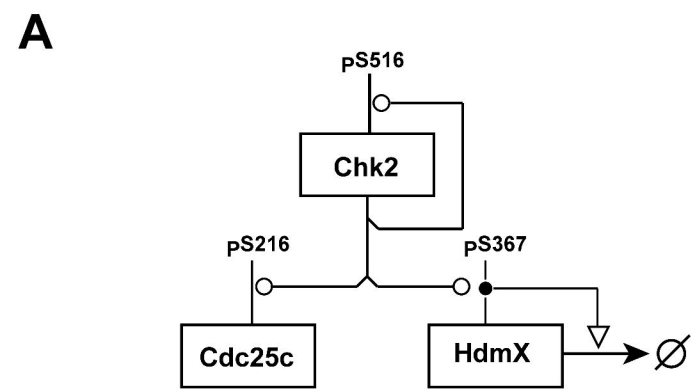
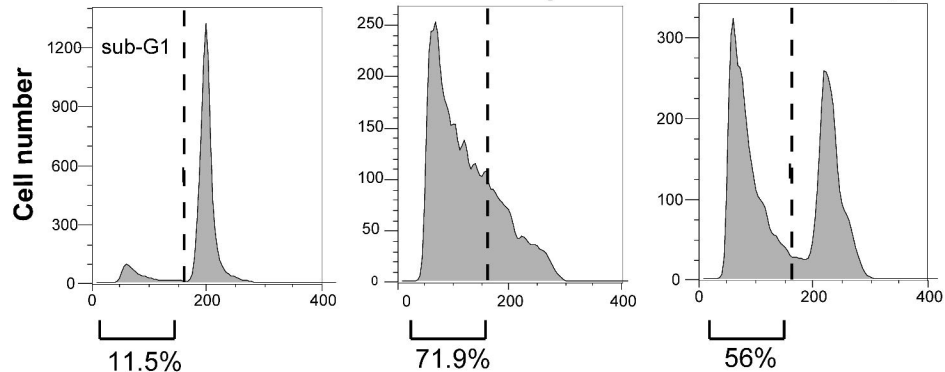
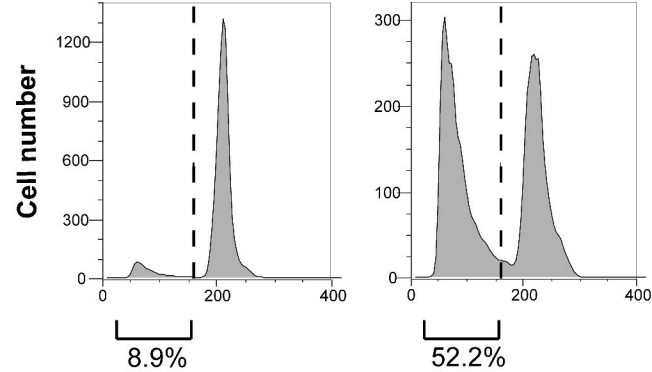
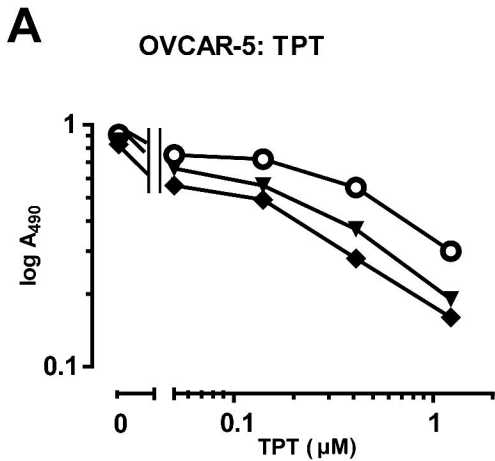


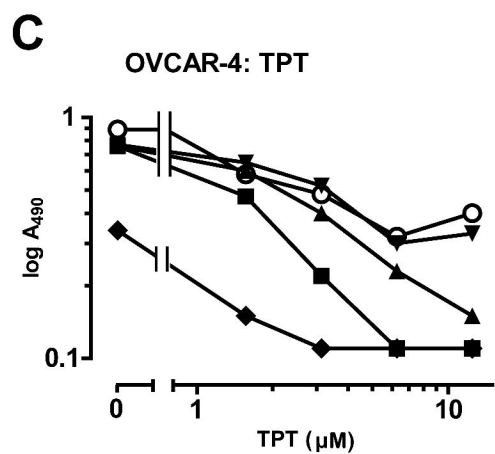
Figure 3

A**Chk2 +/+****Control****IR- 5Gy****IR + PV1019 1 μ M****B****Chk2 -/-****Control****IR - 5Gy****Figure 4**



B Combination Index (CI) values for PV1019 and TPT in OVCAR-5 cells

		TPT μM		
		0.1	0.4	1.2
PV1019 μM	3	0.56	0.45	0.32
	6	0.75	0.59	0.38
	12.5	0.80	0.69	0.44
	25	0.77	0.52	0.43



D Combination Index (CI) values for PV1019 and TPT in OVCAR-4 cells

		TPT μM		
		3.1	6.3	12.5
PV1019 μM	12.5	0.50	0.34	0.48
	23	0.45	0.50	0.43

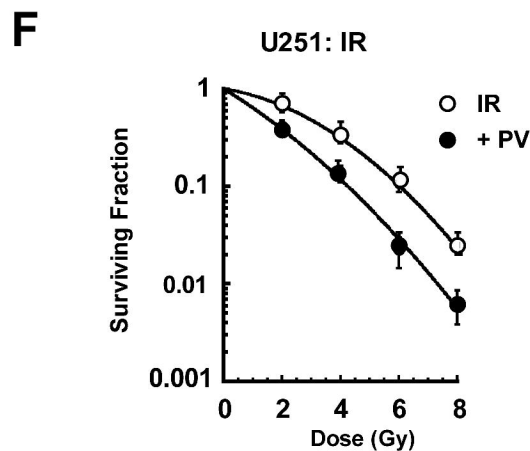
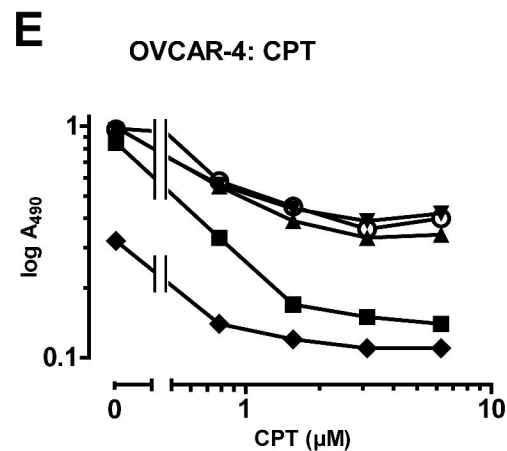


Figure 5

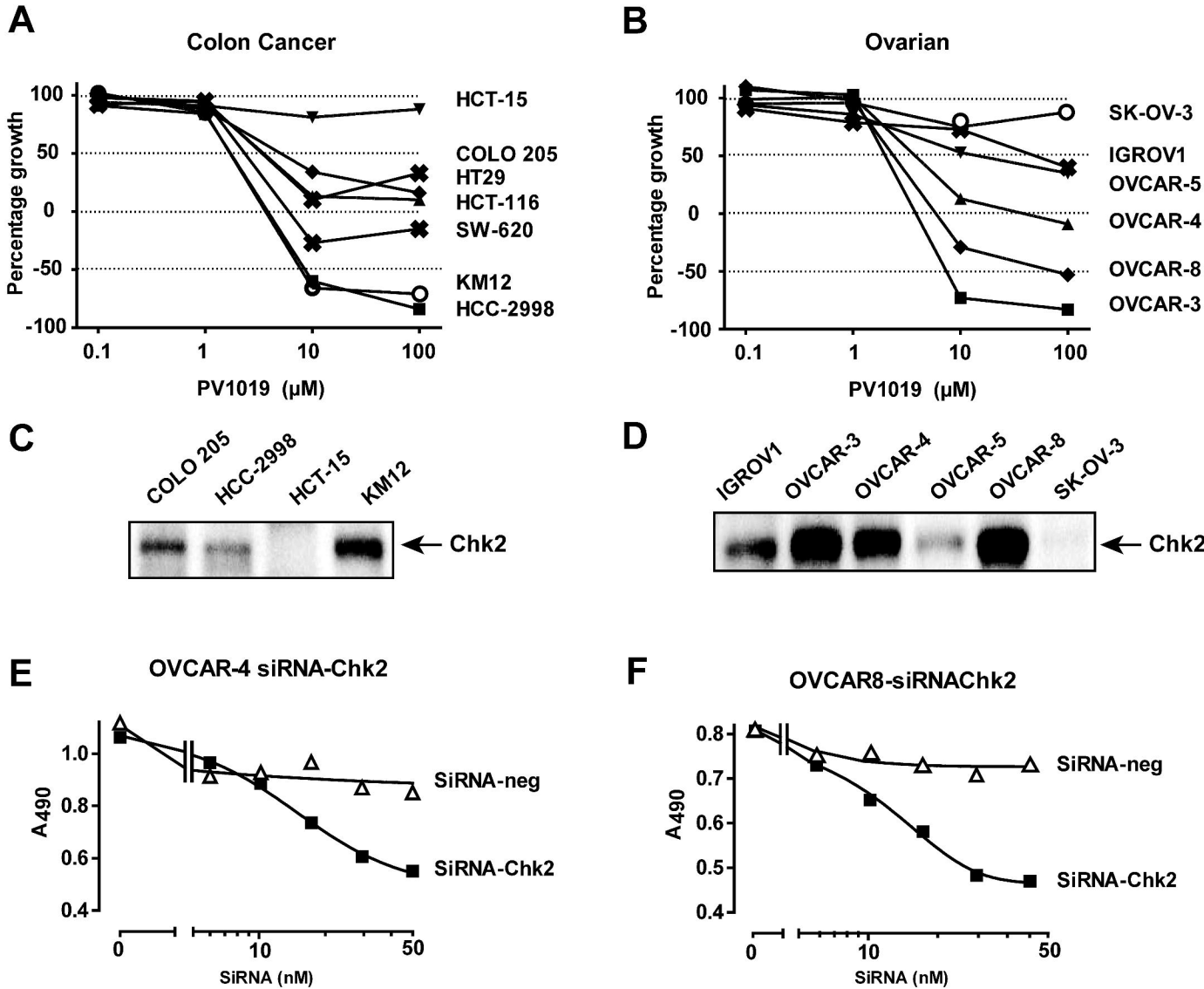


Figure 6